A Simple F–Test Based Multi-Antenna Spectrum Sensing Technique

Tilahun M. Getu[†‡], Wessam Ajib[‡], and René Jr. Landry[†]
[†]École de Technologie Supérieure (ÉTS), Montréal, QC, Canada
[‡]Université du Québec à Montréal (UQÀM), Montréal, QC, Canada
tilahun-melkamu.getu.1@ens.etsmtl.ca, ajib.wessam@uqam.ca, and renejr.landry@etsmtl.ca

***Abstract*—An F–test detector with a simple analytical false alarm threshold expression is considered an alternative to the blind detectors which exhibit complicated analytical expressions. However, the existing F–test requires the channel state information (CSI) as a prior knowledge implicating its sensitivity to CSI estimation error. In this paper, we present and evaluate the performance of a simple F–test based spectrum sensing technique that doesn't require the knowledge of the CSI for a multi-antenna cognitive radio. For this detector, exact and asymptotic analytical performance closed-form expressions are derived. Simulations assess the performance of the presented detector and validate the derived closed-form expressions.**

***Index Terms*—Cognitive radio, spectrum sensing, channel state information, F–test.**

I. Introduction

Cognitive radio (CR) is a promising technology to alleviate the problem of spectrum scarcity which is getting aggravated by an ever-increasing demand for higher data rates. To realize such a radio, licensed spectrum sharing techniques such as *spectrum underlay* and *spectrum overlay* have been proposed [1], [2]. In spectrum underlay, a secondary user (SU) is allowed to transmit on the licensed band of a primary user (PU) while respecting a PU's interference threshold [2]. In spectrum overlay, SUs rather transmit after locating idle frequency bands, licensed to PUs, until a primary transmission is conducted on them [2], [3]. Such an idle frequency band detection is called spectrum sensing and hence fundamental to CR based communication systems. As per the bandwidth of the signal to be detected, spectrum sensing techniques can be *narrowband* or *wideband* [4]–[7]. The wideband techniques can be Nyquist based or sub-Nyquist based depending on the adopted sampling rate [6], [8]. Sub-Nyquist sampling techniques usually deploy either compressive sampling [9] or multi-coset sampling [10]. On the other hand, Nyquist based wideband sensing techniques are based on either fast Fourier transforms [11], wavelets [12], or filter-banks [13].

Delving into narrowband sensing, several narrowband spectrum sensing techniques have been proposed over the years [2], [4], [8], [14]. The conventional ones are energy detection (ED) [15]–[17], matched filtering [18], feature-based detection [19], polarization detection [20], sample covariance matrix (SCM) based algorithms [21]–[24], moment ratio detection [25], and max-min detection [26], [27]. Nevertheless, ED relies on the known power spectral density of the noise and exhibits a high sensitivity to noise uncertainty [2], [14] leading to a poor performance at a low signal-to-noise ratio (SNR) regardless of the number of intercepted samples, as demonstrated via *SNR walls* [28]; matched filters suffer from intrinsic computational complexity and hence are unattractive for practical spectrum sensing applications; particular features need to be introduced to deploy feature detectors in OFDM-based communications [2]; polarization detectors are computationally complex and sensitive to estimation errors [20]; SCM-based techniques suffer from performance loss under sample-starved settings—despite their blindness—and their asymptotic threshold differs considerably from the exact value for finite sensors and samples, as attested by [21]; a moment ratio detection is computationally complex and relies on the asymptotic Gaussian distribution; and max-min detector suffer from huge computational complexity.

Apart from the highlighted conventional algorithms, some other algorithms such as Bartlett estimate-based energy detection [29], a frequency domain eigenvalue-based spectrum sensing algorithms [30], subband energy-based spectrum sensing algorithm [31], energy detection spectrum sensing under RF imperfections and with multiple PUs [32], [33], and a robust estimator-correlator and a robust generalized likelihood detectors [34] have been proposed. However, all these important contributions are less attractive for practical CR applications since they rely on the complex Gaussian distributed primary signal. Recently, the F–test based spectrum sensing technique was proposed in [35] and corroborated to be superior over an energy detector, a maximum-minimum eigenvalue (MME) detector [22], and a generalized likelihood ratio test (GLRT) detector [36], [37], especially at low SNR. While exhibiting a moderate computational complexity, it is also robust against noise uncertainty and independent of noise power. However, it requires a prior knowledge of the channel state information (CSI) between the primary transmitter and secondary receiver rendering it susceptible to CSI estimation errors.

Inspired by the F–test (FT) detector of [35], this paper presents the F–test based blind detector which doesn't require the knowledge of the channel state information (CSI) nor the noise power. In particular, the contributions of this paper are itemized below.

- For a multi-antenna spectrum sensing over flat fading channels, a detector named F–test via singular value decomposition (FT-v-SVD) is presented.
- By using the estimation theory of a population covariance

978-1-5386-6358-5/18/$31.00 ©2018 IEEE

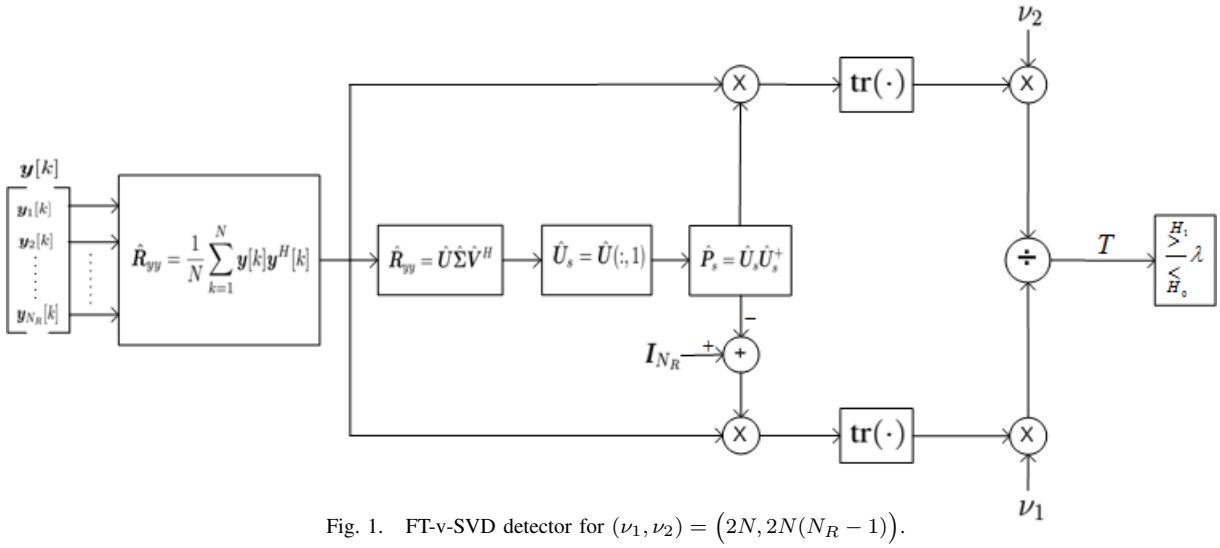

Fig. 1. FT-v-SVD detector for $(\nu_1, \nu_2) = \big(2N, 2N(N_R - 1)\big)$.

matrix (PCM) and F–distributions, the exact and asymptotic performance analyses of FT-v-SVD are reported.

- The performance of FT-v-SVD is assessed through Monte-Carlo simulations which also validate the derived analytical expressions.

Following this introduction, Sec. II presents the notation and system model. Sec. III details the FT-v-SVD algorithm whose performance analyses are presented in Sec. IV. Sec. V reports the simulation results leading to conclusions drawn in Sec. VI.

II. Notation and System Model

A. Notation

Scalars, vectors, and matrices are denoted by italic letters, lower-case boldface letters, and upper-case boldface letters, respectively; $\sim$, $\propto$, $||\cdot||$, $\mathbb{C}^{N_R}$, and $\mathbb{H}^{N_R \times N_R}$ mean distributed as, statistically equivalent, the Euclidean norm, the sets of N_R–dimensional vectors of complex numbers, and of $N_R \times N_R$ Hermitian matrices, respectively; lim, $(\cdot)^T$, $(\cdot)^H$, $(\cdot)^+$, and $\mathcal{CN}_{N_R}(\mathbf{0}, \boldsymbol{\Sigma})$ imply limit, transpose, Hermitian, the Moore-Penrose inverse, and a zero mean circularly symmetric complex additive white Gaussian noise (AWGN) with a covariance matrix of $\boldsymbol{\Sigma}$, respectively; $\Pr\{\cdot\}$, $\text{tr}(\cdot)$, $\text{diag}(\cdot)$, $\boldsymbol{A}(:, j)$, $\boldsymbol{A}(:, i:j)$, and $\boldsymbol{I}_{N_R}$ denote the probability of, trace, diagonal matrix, the jth column of $\boldsymbol{A}$, the columns of $\boldsymbol{A}$ between its ith and jth columns including its ith and jth columns, and an $N_R \times N_R$ identity matrix, respectively; χ^2, F_{ν_1,ν_2}, $F'_{\nu_1,\nu_2}(\lambda_1)$, and $F''_{\nu_1,\nu_2}(\lambda_1, \lambda_2)$ denote chi-square, the central F–distribution with (ν_1, ν_2) degrees of freedom (DoF), the singly non-central F–distribution with (ν_1, ν_2) DoF and non-centrality parameter (NCP) λ_1, and the doubly non-central F–distribution with (ν_1, ν_2) DoF and NCPs (λ_1, λ_2), respectively; and $F(\lambda; \nu_1, \nu_2)$, $F'(\lambda; \nu_1, \nu_2|\lambda_1)$, and $F''(\lambda; \nu_1, \nu_2|\lambda_1, \lambda_2)$ implicate the cumulative distribution function (CDF) of F_{ν_1,ν_2}, the CDF of $F'_{\nu_1,\nu_2}(\lambda_1)$, and the CDF of $F''_{\nu_1,\nu_2}(\lambda_1, \lambda_2)$, respectively, evaluated at λ.

B. System Model

Consider a CR communication system made of a single-antenna primary transmitter and a secondary receiver with N_R antennas. For an opportunistic transmission, the SU senses the licensed band of a PU. Toward this end, a binary hypothesis test is formulated on a primary signal detection as

$$\boldsymbol{y}[k] = \begin{cases} \boldsymbol{h}s[k] + \boldsymbol{z}[k] & : H_1 \\ \boldsymbol{z}[k] & : H_0, \end{cases} \tag{1}$$

where H_0 and H_1 are, respectively, hypotheses regarding the PU idleness and activeness, $\boldsymbol{y}[k] \in \mathbb{C}^{N_R}$ is the kth sample received signal vector, $\boldsymbol{z}[k] \sim \mathcal{CN}_{N_R}(\mathbf{0}, \boldsymbol{\Sigma})$ with $\boldsymbol{\Sigma} \in \mathbb{H}^{N_R \times N_R}$, $\boldsymbol{h} = [h_1, h_2, \ldots, h_{N_R}]^T \in \mathbb{C}^{N_R}$ is the flat fading CSI vector assumed constant during the signal interception, and $s[k]$ is the kth unknown and deterministic primary symbol. We assume *independent and identically distributed* (i.i.d.) noises on the N_R antennas such that $\boldsymbol{\Sigma} = \sigma^2 \boldsymbol{I}_{N_R}$.

III. FT-v-SVD: Algorithm

In this section, the FT-v-SVD algorithm is described. First, the SCM is computed using $\boldsymbol{y}[k]$ in (1) as

$$\hat{\boldsymbol{R}}_{yy} = \frac{1}{N}\sum_{k=1}^{N} \boldsymbol{y}[k]\boldsymbol{y}^H[k], \tag{2}$$

where N is the number of intercepted samples. Second, the SVD of the SCM is computed from (2) as

$$\hat{\boldsymbol{R}}_{yy} = \hat{\boldsymbol{U}}\hat{\boldsymbol{\Sigma}}\hat{\boldsymbol{V}}^H = [\hat{\boldsymbol{U}}_s\ \hat{\boldsymbol{U}}_n]\hat{\boldsymbol{\Sigma}}\hat{\boldsymbol{V}}^H, \tag{3}$$

where $\hat{\boldsymbol{\Sigma}} = \text{diag}(\hat{\sigma}_1, \hat{\sigma}_2, \ldots, \hat{\sigma}_{N_R})$, for $\hat{\sigma}_1 \geq \hat{\sigma}_2 \ldots \geq \hat{\sigma}_{N_R}$ being the singular values, $\hat{\boldsymbol{U}}_s = \hat{\boldsymbol{U}}(:, 1)$ is the estimated subspace spanned by the singular vector corresponding to the largest singular value, and $\hat{\boldsymbol{U}}_n = \hat{\boldsymbol{U}}(:, 2 : N_R)$. Third, the projection matrix $\hat{\boldsymbol{P}}_s$ is computed from $\hat{\boldsymbol{U}}_s$ as

$$\hat{\boldsymbol{P}}_s = \hat{\boldsymbol{U}}_s\hat{\boldsymbol{U}}_s^+ = \hat{\boldsymbol{U}}_s\hat{\boldsymbol{U}}_s^H, \tag{4}$$

where $\boldsymbol{U}_s^+ = (\boldsymbol{U}_s^H\boldsymbol{U}_s)^{-1}\boldsymbol{U}_s^H$ and $\boldsymbol{U}_s^H\boldsymbol{U}_s = 1$ is exploited, as $\hat{\boldsymbol{U}}_s$ is an orthonormal vector.

Fourth, the F–test based decision statistic T and its respective decision rule are defined following [35, eq. (5)] as

$$T \triangleq \frac{\nu_2}{\nu_1} \frac{\text{tr}(\hat{\boldsymbol{P}}_s\hat{\boldsymbol{R}}_{yy})}{\text{tr}\big((\boldsymbol{I}_{N_R} - \hat{\boldsymbol{P}}_s)\hat{\boldsymbol{R}}_{yy}\big)} \underset{H_0}{\overset{H_1}{\gtrless}} \lambda, \tag{5}$$

where $(\nu_1, \nu_2) = (2N, 2N(N_R - 1))$ are the DoF and λ is a decision threshold chosen to satisfy a target false alarm rate (FAR). As a summary, Fig. 1 depicts the FT-v-SVD detector.

Remark 1: Unlike [35, eq. (5)], (5) is independent of the knowledge of the CSI between the primary transmitter and the secondary receiver.

IV. Performance Analyses

Substituting (1) into (2) and, in turn, into (5),

$$T|H_1 = \frac{\nu_2}{\nu_1}\frac{F_1|H_1}{F_2|H_1}, \tag{6}$$

where $F_1|H_1 = \sum_{k=1}^{N}\big(\boldsymbol{h}s[k] + \boldsymbol{z}[k]\big)^H \hat{\boldsymbol{P}}_s\big(\boldsymbol{h}s[k] + \boldsymbol{z}[k]\big)$, $F_2|H_1 = \sum_{k=1}^{N}\big(\boldsymbol{h}s[k] + \boldsymbol{z}[k]\big)^H\big(\boldsymbol{I}_{N_R} - \hat{\boldsymbol{P}}_s\big)\big(\boldsymbol{h}s[k] + \boldsymbol{z}[k]\big)$, and $\boldsymbol{z}[k] \sim \mathcal{CN}_{N_R}(\boldsymbol{0}, \sigma^2\boldsymbol{I}_{N_R})$. As $T|H_1$ is the ratio of two non-central χ^2–distributed random variables (RVs), $T|H_1 \sim F''_{\nu_1,\nu_2}(\lambda_1^{H_1}, \lambda_2^{H_1})$ [35], where $\big(\lambda_1^{H_1}, \lambda_2^{H_1}\big) = \frac{2}{\sigma^2}\sum_{k=1}^{N}\big(\big|\big|\hat{\boldsymbol{P}}_s\boldsymbol{h}s[k]\big|\big|^2, \big|\big|\big(\boldsymbol{I}_{N_R} - \hat{\boldsymbol{P}}_s\big)\boldsymbol{h}s[k]\big|\big|^2\big)$. Similarly, the test statistic under H_0 is given by

$$T|H_0 = \frac{\nu_2}{\nu_1}\frac{F_1|H_0}{F_2|H_0}, \tag{7}$$

where $F_2|H_0 = \sum_{k=1}^{N}\boldsymbol{z}[k]^H(\boldsymbol{I}_{N_R} - \hat{\boldsymbol{P}}_s)\boldsymbol{z}[k]$ and $F_1|H_0 = \sum_{k=1}^{N}\boldsymbol{z}[k]^H\hat{\boldsymbol{P}}_s\boldsymbol{z}[k]$. The right-hand-side of (7) is a ratio of two central χ^2–distributed RVs. Thus, $T|H_0 \sim F_{\nu_1,\nu_2}$ [35].

The exact $P_f = \Pr\{T|H_0 > \lambda\}$ exhibited by FT-v-SVD becomes

$$P_f = 1 - \Pr\big\{T|H_0 \le \lambda\big\} = 1 - F\big(\lambda; \nu_1, \nu_2\big). \tag{8}$$

Similarly, the exact P_d for a given λ can be computed as

$$P_d = \Pr\big\{T|H_1 > \lambda\big\} = 1 - \Pr\big\{T|H_1 \le \lambda\big\}. \tag{9}$$

Since $T|H_1 \sim F''_{\nu_1,\nu_2}(\lambda_1^{H_1}, \lambda_2^{H_1})$, (9) simplifies to

$$P_d = 1 - F''\big(\lambda; \nu_1, \nu_2\big|\lambda_1^{H_1}, \lambda_2^{H_1}\big). \tag{10}$$

For infinitely large samples, the estimation theory of a PCM corroborates that the SCM perfectly approximates the PCM. Accordingly, the asymptotic P_d with respect to (w.r.t.) N is characterized via the following theorem.

Theorem 1:

$$\lim_{N\to\infty} P_d = 1 - F'(\lambda; \nu_1, \nu_2|\lambda^{H_1}), \tag{11}$$

where $\lambda^{H_1} = \lim_{N\to\infty}\frac{2}{\sigma^2}\sum_{k=1}^{N}\big|\big|\boldsymbol{h}s[k]\big|\big|^2$. For $\bar{\gamma}_{snr}^{\infty} = \lim_{N\to\infty}\frac{1}{N}\sum_{k=1}^{N}\frac{\big|\big|\boldsymbol{h}s[k]\big|\big|^2}{N_R\sigma^2}$ being the average SNR over an infinite duration, $\lim_{N\to\infty} P_d = 0$ provided that $\lambda > (N_R - 1)\bar{\gamma}_{snr}^{\infty}$.

Proof: As $N \to \infty$, the SCM perfectly estimates the PCM. Thus, for $\boldsymbol{U} = [\boldsymbol{U}_s\ \boldsymbol{U}_n]$ and $\boldsymbol{U}_s = \boldsymbol{U}(:, 1)$ being the true primary subspace,

$$\lim_{N\to\infty}\big[\hat{\boldsymbol{R}}_{yy}, \hat{\boldsymbol{P}}_s\big] = \big[\boldsymbol{R}_{yy} = [\boldsymbol{U}_s\ \boldsymbol{U}_n]\boldsymbol{\Sigma}\boldsymbol{V}^H, \boldsymbol{P}_s = \boldsymbol{U}_s\boldsymbol{U}_s^{+}\big]. \tag{12}$$

Applying limit and its properties to (6) and, in turn, to (9), and deploying the property of the perfect projector $\boldsymbol{P}_s$ render (11). Moreover, employing (12) in $\lim_{N\to\infty} T|H_1$ and expanding result in $\lim_{N\to\infty} T|H_1 = (N_R - 1)\bar{\gamma}_{snr}^{\infty}$. Hence, if $\lambda > (N_R - 1)\bar{\gamma}_{snr}^{\infty}$, $\lim_{N\to\infty} P_d = \lim_{N\to\infty}\big\{(N_R - 1)\bar{\gamma}_{snr}^{\infty} > \lambda\big\} = 0$. ■

Similarly, the PCM estimation theory is deployed to characterize the exhibited asymptotic P_f that is stated beneath.

Corollary 1: Whenever $\lambda > 0$,

$$\lim_{N\to\infty} P_f = 0. \tag{13}$$

Proof: Note that $\lim_{N\to\infty} T|H_0 = \lim_{N\to\infty} T|H_1\big|_{\{s[k]\}_{k=1}^{N}=0}$. Thus, $\lim_{N\to\infty} T|H_0 = (N_R - 1)\bar{\gamma}_{snr}^{\infty}\big|_{\{s[k]\}_{k=1}^{N}=0} = 0$ and $\lim_{N\to\infty} P_f = \Pr\{0 > \lambda\}$. Thus, if $\lambda > 0$, $\lim_{N\to\infty} P_f = 0$. ■

Remark 2: As $N \to \infty$, FT-v-SVD exhibits a null probability of false alarm.

V. Simulation Results

Unless otherwise mentioned, the subsequent simulations deploy the parameters of Table I. Without loss of generality and similar to [38], we consider $\boldsymbol{h} \sim \mathcal{CN}_{N_R}(\boldsymbol{0}, \boldsymbol{I}_{N_R})$. Besides, we consider a quadrature phase shift keying (QPSK) modulated primary signal, i.e, $s[k] = \sqrt{P_s/2}\big[s_k^I + js_k^Q\big]$ for P_s being the transmitted power and $\{s_k^I, s_k^Q\} \in \{-1, 1\} \times \{-1, 1\}$. By defining the SNR as $\gamma_{snr} = \big|\big|\boldsymbol{h}s[k]\big|\big|^2/N_R\sigma^2$, FT-v-SVD is simulated via (5). Throughout this section, the test threshold rendering a target FAR of 0.1 is obtained via averaging over 10^6 channel realizations.

Simulation parameters	Assigned value
N_R	5
P_s	10 W
(No. of realizations, N)	$(10^3, 10^3)$

TABLE I
Simulation parameters unless otherwise mentioned.

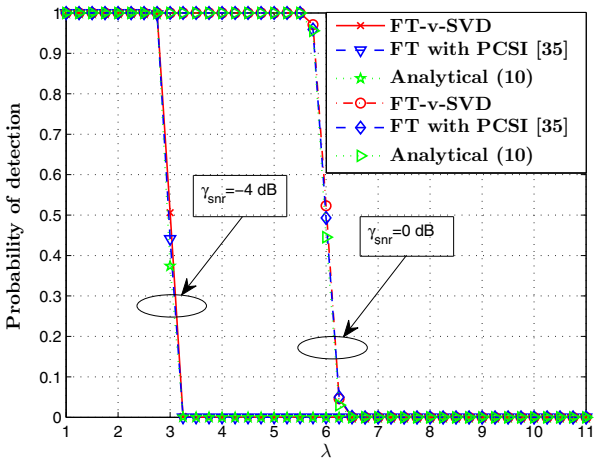

Fig. 2. P_d versus λ.

The detection plots are simulated by assuming the reception of a QPSK signal over frequency flat fading channels. The

false alarm plots are simulated by considering the samples of an AWGN of power σ^2 as an input.

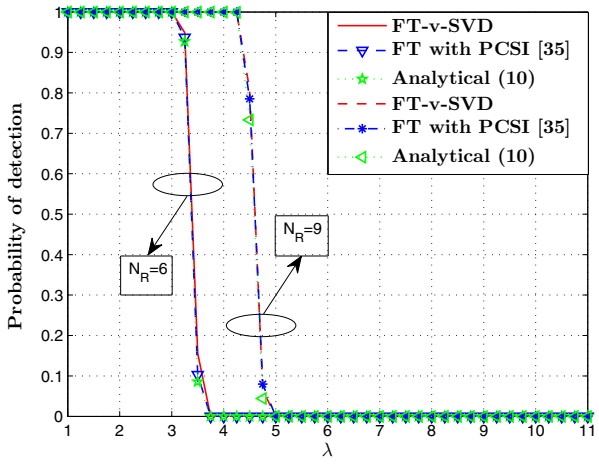

Fig. 3. P_d versus λ: $\gamma_{snr} = -4$ dB.

As observed in Fig. 2, FT-v-SVD which is a blind detector performs as good as the one in [35] fed with a perfect CSI (PCSI) regardless of the SNR. As λ increases, the detection performance of FT-v-SVD falls like FT with PCSI, as both become susceptible of more ambiguity. Fig. 3 corroborates the P_d versus λ plot, w.r.t. a different number of secondary antennas. As before, FT-v-SVD and FT with PCSI manifest identical performance regardless of N_R. Besides, their detection performance improves with the increment of N_R. Meanwhile, Figs. 2 and 3 validate (10) which was plotted via the approximation in [35, eqs. (21) and (22)].

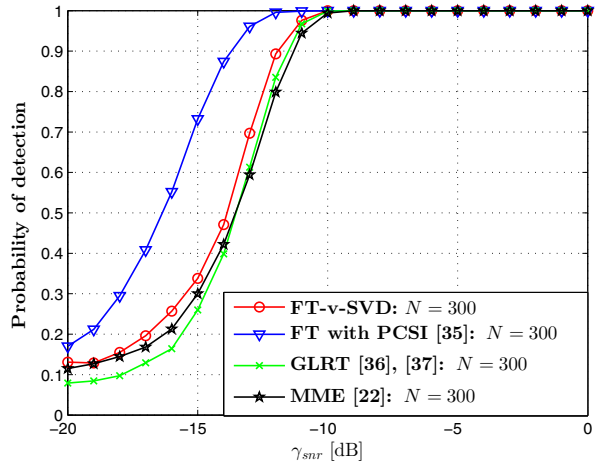

Fig. 4. P_d versus γ_{snr}: $P_f = 0.1$ and 10^4 realizations.

Fig. 4 displays that FT-v-SVD improves both MME [22] and GLRT [36], [37] for the detection of a primary signal manifesting a very low SNR. Moreover, it is corroborated by the same plot that FT-v-SVD—being a blind detector—performs as good as FT [35] fed with a PCSI for $\gamma_{snr} \geq -10$ dB. As N increases from 300 to 600, Fig. 5 demonstrates that the performance of FT-v-SVD approaches that of FT's even

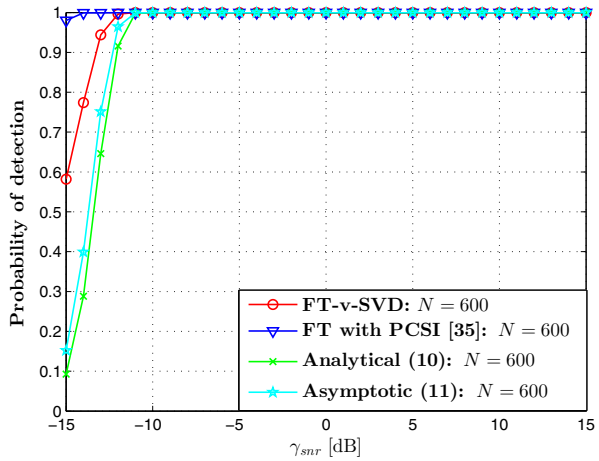

Fig. 5. P_d versus γ_{snr}: $P_f = 0.1$.

at very low SNR. This phenomenon implies that FT-v-SVD exhibits a null probability of false alarm. performs as good as, regardless of the SNR, the detector fed with PCSI when N gets larger. For weak to moderately weak SNR, Fig. 5 validates the accuracy of the exact and asymptotic expressions given by (10) and (11). For $\gamma_{snr} \leq -10$ dB, results of these expressions deviate from the Monte-Carlo simulation results, especially for $N = 300$. This implies that the approximations in [35, eqs. (21) and (22)] that were deployed in the depiction of the results of (10) give poor results. On the other hand, as N increases from 300 to 600, the accuracy of the asymptotic expression increases, regardless of the SNR, implying its validity as N gets larger.

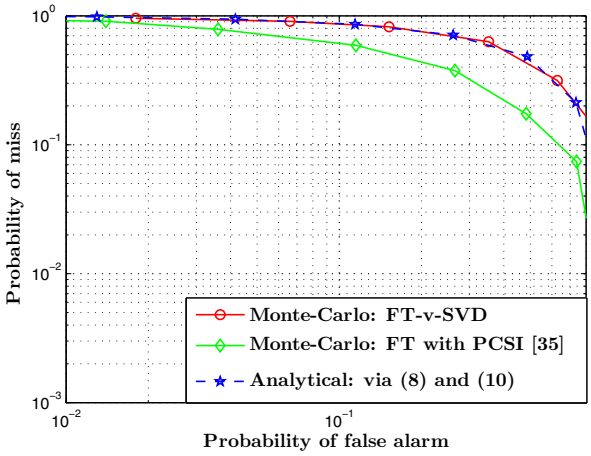

Fig. 6. P_m versus P_f: $N = 50$ and $\gamma_{snr} = -15$ dB.

Fig. 6 depicts the complementary receiver operating characteristics manifested by FT-v-SVD and FT. As evident from Fig. 6, FT with PCSI offers a slightly smaller probability of miss (P_m)—simulated as $P_m = 1 - P_d$—for a given P_f than FT-v-SVD. Such a performance loss is due to a slightly smaller P_d exhibited by FT-v-SVD, especially for N as small as 50. Hence, this is a little price to pay by FT-v-SVD when compared with FT fed with PCSI. Moreover, Fig. 6 validates

(10)—plotted via [35, eqs. (21) and (22)]—and (8).

VI. Conclusions

CR helps to overcome the discrepancy between spectrum underutilization and spectrum scarcity. Such systems employing a spectrum overlay access scheme would be efficient and reliable whenever spectrum holes are efficiently and robustly detected. In this respect, efficient and robust spectrum sensing shall not rely on the presumed noise power nor the primary signal characteristics. Accordingly, simple F–test based blind spectrum sensing technique named FT-v-SVD is presented for a multi-antenna spectrum sensing over flat fading channels. For this detector, exact and asymptotic performance analyses are provided. Simulations conducted using i.i.d. noises assess the performance of the aforementioned detector and validate the derived closed-form expressions.

References

[1] Q. Zhao and B. M. Sadler, "A survey of dynamic spectrum access," *IEEE Signal Process. Mag.*, vol. 24, no. 3, pp. 79–89, May 2007.

[2] B. Wang and K. J. R. Liu, "Advances in cognitive radio networks: A survey," *IEEE J. Sel. Topics Signal Process.*, vol. 5, no. 1, pp. 5–23, Feb. 2011.

[3] S. Haykin, "Cognitive radio: brain-empowered wireless communications," *IEEE J. Sel. Areas Commun.*, vol. 23, no. 2, pp. 201–220, Feb. 2005.

[4] S. K. Sharma, T. E. Bogale, S. Chatzinotas, B. Ottersten, L. B. Le, and X. Wang, "Cognitive radio techniques under practical imperfections: A survey," *IEEE Commun. Surveys Tuts.*, vol. 17, no. 4, pp. 1858–1884, 4th Quart., 2015.

[5] T. E. Bogale, L. Vandendorpe, and L. B. Le, "Wide-band sensing and optimization for cognitive radio networks with noise variance uncertainty," *IEEE Trans. Commun.*, vol. 63, no. 4, pp. 1091–1105, Apr. 2015.

[6] H. Sun, A. Nallanathan, C. X. Wang, and Y. Chen, "Wideband spectrum sensing for cognitive radio networks: A survey," *IEEE Wireless Commun.*, vol. 20, no. 2, pp. 74–81, Apr. 2013.

[7] S. K. Jayaweera, *Signal Processing for Cognitive Radios*, 1st ed. Hoboken, NJ, USA: Wiley, 2014.

[8] A. Ali and W. Hamouda, "Advances on spectrum sensing for cognitive radio networks: Theory and applications," *IEEE Commun. Surveys Tuts.*, vol. 19, no. 2, pp. 1277–1304, 2nd Quart., 2017.

[9] D. L. Donoho, "Compressed sensing," *IEEE Trans. Inf. Theory*, vol. 52, no. 4, pp. 1289–1306, Apr. 2006.

[10] R. Venkataramani and Y. Bresler, "Perfect reconstruction formulas and bounds on aliasing error in sub-Nyquist nonuniform sampling of multiband signals," *IEEE Trans. Inf. Theory*, vol. 46, no. 6, pp. 2173–2183, Sep. 2000.

[11] Z. Quan, S. Cui, A. H. Sayed, and H. V. Poor, "Optimal multiband joint detection for spectrum sensing in cognitive radio networks," *IEEE Trans. Signal Process.*, vol. 57, no. 3, pp. 1128–1140, Mar. 2009.

[12] Z. Tian and G. B. Giannakis, "A wavelet approach to wideband spectrum sensing for cognitive radios," in *Proc. Int. Conf. Cogn. Radio Oriented Wireless Netw. Commun.*, Jun. 2006, pp. 1–5.

[13] B. Farhang-Boroujeny, "Filter bank spectrum sensing for cognitive radios," *IEEE Trans. Signal Process.*, vol. 56, no. 5, pp. 1801–1811, May 2008.

[14] E. Axell, G. Leus, E. G. Larsson, and H. V. Poor, "Spectrum sensing for cognitive radio : State-of-the-art and recent advances," *IEEE Signal Process. Mag.*, vol. 29, no. 3, pp. 101–116, May 2012.

[15] A. Sonnenschein and P. M. Fishman, "Radiometric detection of spread-spectrum signals in noise of uncertain power," *IEEE Trans. Aerosp. Electron. Syst.*, vol. 28, no. 3, pp. 654–660, Jul. 1992.

[16] F. F. Digham, M. S. Alouini, and M. K. Simon, "On the energy detection of unknown signals over fading channels," *IEEE Trans. Commun.*, vol. 55, no. 1, pp. 21–24, Jan. 2007.

[17] P. C. Sofotasios, E. Rebeiz, L. Zhang, T. A. Tsiftsis, D. Cabric, and S. Freear, "Energy detection based spectrum sensing over $\kappa-\mu$ and $\kappa-\mu$ extreme fading channels," *IEEE Trans. Veh. Technol.*, vol. 62, no. 3, pp. 1031–1040, Mar. 2013.

[18] H. V. Poor, *An Introduction to Signal Detection and Estimation*. New York, NY, USA: Springer-Verlag, 1994.

[19] W. A. Gardner, "Signal interception: a unifying theoretical framework for feature detection," *IEEE Trans. Commun.*, vol. 36, no. 8, pp. 897–906, Aug. 1988.

[20] C. Guo, S. Chen, and F. Liu, "Polarization-based spectrum sensing algorithms for cognitive radios: Upper and practical bounds and experimental assessment," *IEEE Trans. Veh. Technol.*, vol. 65, no. 10, pp. 8072–8086, Oct. 2016.

[21] A. Kortun, M. Sellathurai, T. Ratnarajah, and C. Zhong, "Distribution of the ratio of the largest eigenvalue to the trace of complex Wishart matrices," *IEEE Trans. Signal Process.*, vol. 60, no. 10, pp. 5527–5532, Oct. 2012.

[22] Y. Zeng and Y.-C. Liang, "Eigenvalue-based spectrum sensing algorithms for cognitive radio," *IEEE Trans. Commun.*, vol. 57, no. 6, pp. 1784–1793, Jun. 2009.

[23] Y. Zeng and Y. C. Liang, "Spectrum-sensing algorithms for cognitive radio based on statistical covariances," *IEEE Trans. Veh. Technol.*, vol. 58, no. 4, pp. 1804–1815, May 2009.

[24] P. Bianchi, M. Debbah, M. Maida, and J. Najim, "Performance of statistical tests for single-source detection using random matrix theory," *IEEE Trans. Inf. Theory*, vol. 57, no. 4, pp. 2400–2419, Apr. 2011.

[25] T. E. Bogale and L. Vandendorpe, "Moment based spectrum sensing algorithm for cognitive radio networks with noise variance uncertainty," in *Proc. Annu. Conf. on Inform. Sci. and Syst. (CISS)*, Mar. 2013, pp. 1–5.

[26] ——, "Max-min SNR signal energy based spectrum sensing algorithms for cognitive radio networks with noise variance uncertainty," *IEEE Trans. Wireless Commun.*, vol. 13, no. 1, pp. 280–290, Jan. 2014.

[27] ——, "Linearly combined signal energy based spectrum sensing algorithm for cognitive radio networks with noise variance uncertainty," in *Proc. Int. Conf. on Cognitive Radio Oriented Wireless Networks*, Jul. 2013, pp. 80–86.

[28] R. Tandra and A. Sahai, "SNR walls for signal detection," *IEEE J. Sel. Topics Signal Process.*, vol. 2, no. 1, pp. 4–17, Feb. 2008.

[29] E. H. Gismalla and E. Alsusa, "On the performance of energy detection using Bartlett's estimate for spectrum sensing in cognitive radio systems," *IEEE Trans. Signal Process.*, vol. 60, no. 7, pp. 3394–3404, Jul. 2012.

[30] E. Yousif, T. Ratnarajah, and M. Sellathurai, "A frequency domain approach to eigenvalue-based detection with diversity reception and spectrum estimation," *IEEE Trans. Signal Process.*, vol. 64, no. 1, pp. 35–47, Jan. 2016.

[31] S. Dikmese, P. Sofotasios, M. Renfors, and M. Valkama, "Subband energy based reduced complexity spectrum sensing under noise uncertainty and frequency-selective spectral characteristics," *IEEE Trans. Signal Process.*, vol. 64, no. 1, pp. 131–145, Jan. 2016.

[32] A. A. A. Boulogeorgos, N. D. Chatzidiamantis, and G. K. Karagiannidis, "Energy detection spectrum sensing under RF imperfections," *IEEE Trans. Commun.*, vol. 64, no. 7, pp. 2754–2766, Jul. 2016.

[33] ——, "Spectrum sensing with multiple primary users over fading channels," *IEEE Commun. Lett.*, vol. 20, no. 7, pp. 1457–1460, Jul. 2016.

[34] A. Patel, S. Biswas, and A. K. Jagannatham, "Optimal GLRT-based robust spectrum sensing for MIMO cognitive radio networks with CSI uncertainty," *IEEE Trans. Signal Process.*, vol. 64, no. 6, pp. 1621–1633, Mar. 2016.

[35] Q. Huang and P. J. Chung, "An F–test based approach for spectrum sensing in cognitive radio," *IEEE Trans. Wireless Commun.*, vol. 12, no. 8, pp. 4072–4079, Aug. 2013.

[36] A. Taherpour, M. Nasiri-Kenari, and S. Gazor, "Multiple antenna spectrum sensing in cognitive radios," *IEEE Trans. Wireless Commun.*, vol. 9, no. 2, pp. 814–823, Feb. 2010.

[37] P. Wang, J. Fang, N. Han, and H. Li, "Multiantenna-assisted spectrum sensing for cognitive radio," *IEEE Trans. Veh. Technol.*, vol. 59, no. 4, pp. 1791–1800, May 2010.

[38] D. Ramírez, J. Vía, I. Santamaría, and L. L. Scharf, "Detection of spatially correlated Gaussian time series," *IEEE Trans. Signal Process.*, vol. 58, no. 10, pp. 5006–5015, Oct. 2010.